

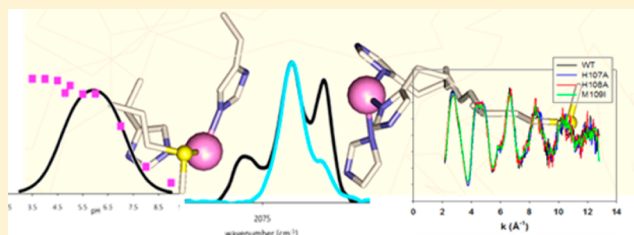
# HMM Motif at the CuH-Site of Peptidylglycine Monooxygenase is a pH-Dependent Conformational Switch

Chelsey D. Kline, Mary Mayfield, and Ninian J. Blackburn\*

Institute of Environmental, Health, Oregon Health and Sciences University, Beaverton, Oregon 97006, United States

## S Supporting Information

**ABSTRACT:** Peptidylglycine monooxygenase is a copper-containing enzyme that catalyzes the amidation of neuropeptides hormones, the first step of which is the conversion of a glycine-extended pro-peptide to its  $\alpha$ -hydroxyglycine intermediate. The enzyme contains two mononuclear Cu centers termed CuM (ligated to imidazole nitrogens of H242, H244 and the thioether S of M314) and CuH (ligated to imidazole nitrogens of H107, H108, and H172) with a Cu–Cu separation of 11 Å. During catalysis, the M site binds oxygen and substrate, and the H site donates the second electron required for hydroxylation. The WT enzyme shows maximum catalytic activity at pH 5.8 and undergoes loss of activity at lower pHs due to a protonation event with a  $pK_A$  of 4.6. Low pH also causes a unique structural transition in which a new S ligand coordinates to copper with an identical  $pK_A$ , manifest by a large increase in Cu–S intensity in the X-ray absorption spectroscopy. In previous work (Bauman, A. T., Broers, B. A., Kline, C. D., and Blackburn, N. J. (2011) *Biochemistry* 50, 10819–10828), we tentatively assigned the new Cu–S interaction to binding of M109 to the H-site (part of an HMM conserved motif common to all but one member of the family). Here we follow up on these findings via studies on the catalytic activity, pH-activity profiles, and spectroscopic (electron paramagnetic resonance, XAS, and Fourier transform infrared) properties of a number of H-site variants, including H107A, H108A, H172A, and M109I. Our results establish that M109 is indeed the coordinating ligand and confirm the prediction that the low pH structural transition with associated loss of activity is abrogated when the M109 thioether is absent. The histidine mutants show more complex behavior, but the almost complete lack of activity in all three variants coupled with only minor differences in their spectroscopic properties suggests that unique structural elements at H are critical for functionality. The data suggest a more general utility for the HMM motif as a copper- and pH-dependent conformational switch.



Mononuclear copper monooxygenases represent a small but important group of metalloenzymes involved in neurotransmitter and peptide hormone biosynthesis. They include the enzymes dopamine  $\beta$ -monooxygenase (DBM)<sup>1</sup> and tyramine  $\beta$ -monooxygenase (TBM)<sup>2</sup> involved in catecholamine biosynthesis, and peptidylglycine monooxygenase (PHM) which catalyzes the amidation of neuropeptide hormones, the first step of which is the conversion of a glycine-extended pro-peptide to its  $\alpha$ -hydroxyglycine intermediate.<sup>3</sup> The active sites of these enzymes appear to be homologous as determined by a combination of crystallographic,<sup>4–8</sup> spectroscopic,<sup>9–13</sup> kinetic,<sup>1,2,14,15</sup> and computational studies,<sup>8,16–18</sup> but PHM remains the only member of the group for which crystal structures are available. The two copper centers termed CuM and CuH are mononuclear and are separated by 11 Å of solvent-filled channel, in contrast to the better characterized dinuclear centers in hemocyanins, tyrosinases,<sup>17,19–21</sup> and oxygen activating models<sup>22,23</sup> in which the Cu–Cu distance is 3–4 Å. A Cu<sub>M</sub>-superoxo intermediate has been suggested on the basis of additional crystallographic<sup>24</sup> and biochemical data,<sup>14,25</sup> while *in silico* studies<sup>16,17</sup> have validated Cu(II)-O<sub>2</sub><sup>•−</sup> as a probable reactive oxygen species. It has been further suggested that the large spatial separation of the Cu centers in PHM prevents immediate formation of the peroxide and thus allows

the potent electrophilic reactivity of the mononuclear Cu(II)-superoxo species to be fully expressed in the form of H-atom abstraction from the substrate<sup>14,16,17</sup> to form a mononuclear hydroperoxo species at Cu<sub>M</sub> and a substrate radical.

The M-site is considered to be the catalytic locus and is coordinated by H242, H244, and solvent ligands in the oxidized form with a weak EXAFS-undetectable interaction with the thioether of M314; on reduction, the solvent ligands dissociate and the thioether S from M314 binds to the Cu(I).<sup>12,13,26</sup> A structure of reduced PHM cocrystallized with a slow substrate has allowed the visualization of a “pre-catalytic complex” involving a dioxygen molecule bound at Cu<sub>M</sub>, the bond length of which is consistent with a Cu(II)-superoxo species. The O–O bond is oriented away from the C–H bond of the substrate which binds nearby, but a facile rotation about the Cu–O bond could bring the distal O and the substrate C–H bond into alignment.<sup>24</sup> The M314 ligand plays a critical role in optimizing the M-site for catalysis since mutation to His, Cys, or Asp results in ~95% loss in activity.<sup>2,27</sup> Whereas the M-site is the

Received: February 21, 2013

Revised: March 25, 2013

Published: March 26, 2013



catalytic center, the H-site is believed to be an electron transfer center responsible for supplying the second electron necessary to complete the monooxygenation reaction. In the resting oxidized protein, Cu<sub>H</sub> is unremarkable with a [(His)<sub>3</sub>(OH<sub>2</sub>)] ligand set, but reduction again induces loss of solvent and generates a Cu(I) site with Cu–N(His) distances more typical of a two-coordinate system (1.88 Å).<sup>26,28,29</sup> The similarity of the extended X-ray absorption fine structure (EXAFS) of the reduced protein in the WT and H172A derivatives suggests that of the three copper-coordinating His residues (107, 108, and 172), H172 is only weakly bound in the reduced protein. Nevertheless, mutation to alanine has a dramatic effect on catalysis with the  $k_{\text{cat}}$  decreasing by 3 orders of magnitude.<sup>15</sup> Furthermore, crystallographic analysis reveals a structural interaction between the M and H sites, with the M314I inducing dissociation of the H107 ligand from the H-center, some 11 Å distant.<sup>6</sup> H172 forms a stacking interaction with the conserved Y79 residue, and it has been suggested from studies on the related enzyme TBM<sup>30</sup> that the H172 ligand might form the exit pathway for the electron as it transfers from H to M using Y79 and oriented water molecules as additional elements of the ET pathway.<sup>31</sup>

WT PHM shows maximum catalytic activity at pH 5.8 and undergoes loss of activity at lower pHs due to a protonation event with a  $pK_A$  of 4.6. Low pH also causes a unique structural transition in which a new S ligand coordinates to copper with an identical  $pK_A$ , manifest by a large increase in Cu–S intensity in the XAS. In previous work we tentatively assigned the new Cu–S interaction to binding of M109 to the H-site (part of the HHM conserved motif common to all but one member of the family), induced by protonation of one of the H-site histidine residues.<sup>27</sup> These data suggested that the H-site is also conformationally mobile and hint at allosteric gating of ET via long-range structural perturbations. In the present paper we follow up on these findings via studies on the catalytic activity, pH-activity profiles, and spectroscopic properties of a number of H-site variants, including H107A, H108A, H172A, and M109I. Our results establish that M109 is indeed the coordinating ligand and confirm the prediction that this mutant should show no decrease in activity at low pH. The histidine mutants show more complex behavior, but the almost complete lack of activity in all three variants coupled with only minor changes in spectroscopic properties suggests that unique structural elements at H are critical for functionality.

## MATERIALS AND METHODS

Buffers and ascorbate were obtained from Sigma-Aldrich at a minimum purity of 99%. Beef liver catalase was acquired from Roche. Substrates Ac-Tyr-Val-Gly (Ac-YVG) and dansyl-Tyr-Val-Gly (dansyl-YVG) were purchased from Peptide International and American Peptide Co, respectively.

**Construction of PHMcc CuH site Mutants.** WT, H172A, and H107A PHMcc were constructed as previously reported.<sup>32,33</sup> PHMcc mutants (H108A and M109I) were individually introduced into pBS.ΔProPHM382s (obtained as a gift from Betty A. Eipper and Richard E. Mains) using Splicing by Overlap Extension (SOEing).<sup>32,34</sup> Sense and antisense oligonucleotide primers (Table S1) encoding about 15 bases downstream and upstream of the mutation were used for site-directed mutagenesis and paired with primers upstream and downstream of two restriction enzyme sites, ClaI & XbaI. PCR products were purified on agarose gels. Final PCR products were phenol-chloroform extracted, digested using

restriction enzymes (NEB), fractionated on agarose gels, purified via Qiagen PCR kit, and then ligated into the pCIS.2CXXNH expression vector (also a gift from Betty A. Eipper and Richard E. Mains). Sequence analysis was performed on mutant clones, and Qiagen midi prep was used to ensure 20 μg/20 μL of recombinant DNA for transfection.

**Screening PHMcc CuH Site Mutants.** CHO DG44 cells were transfected with the recombinant DNA using Lipofectamine 2000 (Invitrogen). The transfected cells were subsequently selected for *Dhfr* cell lines in  $\alpha$ -minimum Eagle's medium containing 10% dialyzed fetal bovine serum.<sup>33,35</sup> Only those cells that retained the *Dhfr* gene (colocated with PHM on the plasmid) were capable of growth under these conditions. Monoclonal cell lines were created by serial dilution into 96-well plates, in order to select for wells which contained single-cell colonies. These were passed individually into a fresh 96 well, grown to confluence, and screened via Western blot for PHMcc production under similar conditions. The strongest producers were inoculated into a Hollow Fiber Bioreactor with 5 MWCO (Fibercell Systems, Inc.).

**Western Blot Analysis.** CHO DG44 cells were incubated in DMEM/F12 containing 0.5% Fetal Clone II (FCII, Fisher) for at least 24 h before a sample was collected, which was then combined with SDS, and heated for 5 min at 100 °C. Each sample was separated by 8–25% SDS-PAGE and then transferred to an Immobilon P membrane (Millipore) using the PhastSystem. PHM proteins were visualized using rabbit antibody 246 [rPAM(116–131)]<sup>36</sup> diluted 1:1500, and secondary antibody-antirabbit IgG (Sigma) diluted 1:1000, followed by an AP Conjugate Substrate kit (Bio-Rad Laboratories).

**PHMcc Expression and Purification.** Variant cell-lines WT, H107A, and H172A (kindly provided to us by Richard E. Mains and Betty A. Eipper), and H108A and M109I (constructed in house) were grown as described previously.<sup>26,37</sup> Briefly, the stably transfected cell lines were thawed from freezer stock into a T75 flask with 20 mL of DMEM/F12 medium containing 10% FCII serum (Fisher). At 80% confluence the cells were passed into five NUNC triple flasks (500 cm<sup>2</sup> area per flask) which were also grown to confluence. Cells were trypsinized and resuspended in 50 mL of medium with 10% FCII serum prior to inoculation into the extracapillary space (ECS) of a Hollow Fiber Bioreactor (Fibercell Systems 4300-C2008, MWCO 5 kD, 3000 cm<sup>2</sup> surface area) precultured with 2 L of 50 mM PBS pH 7.35 and 2 L of DMEM/F12 10% FCII serum.<sup>26,37,38</sup>

Individual bioreactors containing each of the variants were fed with DMEM/F12/10% FCII serum for a month, after which the serum level was reduced to 0.5% FCII serum.<sup>38</sup> At this point, the bioreactors were fed with 0.5% serum-containing medium every other day, and spent medium (20 mL) from the ECS was collected and frozen at –20 °C for later purification. About a month's worth of bioreactor harvest (300 mL) for each variant was purified as previously described.<sup>38</sup>

**PHMcc Copper Reconstitution.** Purified enzyme was dialyzed against 20 mM sodium phosphate buffer, pH 8.0, and then reconstitution with cupric sulfate by slow addition of 2.5 mol equiv Cu(II) per protein followed by two cycles of dialysis to remove unbound cupric ions. Concentrations were determined using OD<sub>280</sub>(1%) = 0.980 on a Cary 50 spectrophotometer. Copper concentrations were determined using a Perkin-Elmer Optima 2000 DV inductively coupled plasma optical emission spectrometer.

**Specific Activity Measurements.** Enzymatic activity was measured by monitoring oxygen consumption in a Rank Brother's oxygen electrode at 37 °C, as previously reported.<sup>39</sup> Each reaction was performed in a water-jacketed vessel in 2 mL of total volume containing 100 mM MES pH 5.5, 200  $\mu$ L of a 6 mg/mL catalase solution (47 000 units per mg), 100  $\mu$ L of 100  $\mu$ M Cu(II) solution, 10  $\mu$ L of 2 M stock ascorbate, and 80  $\mu$ M dansyl-YVG substrate. In some cases, various concentrations of imidazole up to 10 mM were added in an attempt to rescue activity. The reaction was allowed to equilibrate for approximately 1 min, the reaction vessel was capped, and a baseline was measured for 50 s prior to initiation of the reaction. The reaction was initiated by addition of 10–20  $\mu$ L of enzyme (concentrations varied depending on the activity of the particular variant) through the cap using a Hamilton syringe. The oxygen consumption was monitored and analyzed as previously reported.<sup>27,39</sup> Steady state kinetic measurements were performed as above, varying concentrations of dansyl-YVG between 2.5 and 400  $\mu$ M. Kinetic constants were determined by fitting raw data to the Michaelis–Menten equation using nonlinear regression. Similar assay conditions were used for the measurement of pH–activity profiles in the pH range 3–9, except that a mixed buffer system was employed containing equal volumes of 100 mM each of MES, HEPES, CHES, and formic acid adjusted to the desired pH with sodium hydroxide.

**Coupling of Oxygen and Product.** Coupling of oxygen consumption to product formation was determined for each mutant using HPLC to determine substrate consumed, and the O<sub>2</sub>-electrode to determine oxygen consumed at 37 °C. A reverse phase HPLC Varian Pro Star solvent delivery module was utilized to separate and quantify substrate consumption and product accumulation as previously reported.<sup>27</sup> Reactions were performed in a water-jacketed glass reaction vessel, under similar reaction conditions as for the specific activity measurements (substrate and enzyme concentrations were adjusted for each experiment). The reactants were allowed to equilibrate for 1 min prior to initiating the reaction with enzyme. An aliquot of 200  $\mu$ L from the reaction vessel was removed and quenched with 20  $\mu$ L of 20% TFA after 150–200 s of reaction time. (In the case of M109I, an aliquot of 200  $\mu$ L from the reaction vessel was removed and quenched with 200  $\mu$ L of 20% TCA in order to quench the reaction.) Substrate and product were separated via HPLC, and concentrations were determined using a standard curve of 10–250  $\mu$ M dansyl-YVG run under the same conditions.<sup>27,39</sup> Micromoles oxygen consumed were determined by subtracting the O<sub>2</sub> concentrations at the time of sampling from the value immediately before reaction initiation.

**XAS Samples.** Oxidized samples were prepared in a single step by 5-fold dilution of 2 mM protein in 20 mM phosphate pH 8.0 (4 mM in Cu (II)) with the appropriate mixed buffer containing 20% ethylene glycol.<sup>27</sup> Reduced protein samples were prepared under anaerobic conditions by 5-fold dilution of a 2 mM protein (4 mM in Cu(II) sample of the oxidized enzyme with the appropriate buffer containing 5 mM ascorbate and 20% ethylene glycol. Samples were transferred to an XAS cuvette via a syringe and flash frozen in liquid nitrogen. Final PHMcc copper concentrations ranged from 600 to 1200  $\mu$ M.

**Collection and Analysis of XAS Data.** Copper K-edge (8.9 keV) extended X-ray absorption fine structure (EXAFS) and X-ray absorption near edge structure (XANES) data were collected at the Stanford Synchrotron Radiation Lightsource

operating at 3 GeV with currents between 300 and 450 mA maintained by continuous top-up. Samples were measured on beamline 7–3 using a Si[220] monochromator and a Rh-coated mirror upstream with 13 keV energy cutoff in order to reject harmonics. Data were collected in fluorescence mode using a high-count rate Canberra 30-element Ge array detector with maximum count rates per array element less than 120 kHz. A Z-1 nickel oxide filter and Soller slit assembly inserted in front of the detector was used to reduce elastic scattering relative to the Cu K $\alpha$  fluorescence. Four to six scans of a sample containing only buffer were averaged and subtracted from the averaged data for each protein sample to remove the Ni K $\beta$  fluorescence and produce a flat pre-edge baseline. Samples were measured as aqueous glasses in 20% ethylene glycol at 10 K. Output from each detector channel was inspected for glitches and dropouts before inclusion in the final average.

Data reduction and background subtractions were performed using the program modules of EXAFSPAK.<sup>40</sup> Spectral simulation was carried out using EXCURVE version 9.2<sup>41–43</sup> as described previously.<sup>26</sup> Simulations of the EXAFS data used a mixed-shell model consisting of imidazole from histidines residues and S (Met) coordination. The threshold energy,  $E_0$ , was chosen at 8985 eV, and refinement of structural parameters included distances ( $R$ ), coordination numbers ( $N$ ), and Debye–Waller factors ( $2\sigma^2$ ), and included multiple scattering contributions from outer-shell atoms of imidazole rings.

**CO Binding.** Purified PHMcc was concentrated to approximately 2 mM (4 mM in copper) in 20 mM phosphate pH 8.0, and pH-adjusted with 4 vol of 50 mM mixed buffer MES/HEPES/CHES/formate at either pH 3.5 or 7.5 in a septum-sealed conical vial. Samples were purged with CO before the addition of a 5-fold excess (5 mM) of anaerobic buffered ascorbate and then incubated under an atmosphere of pure CO for 10–15 min. The carbonylated protein solutions were loaded into the IR cell (50 micron pathlength) at a final concentration of 500  $\mu$ M (1 mM in copper). After the protein data were collected, the cell was flushed with buffer and remeasured to collect a baseline. FTIR data were recorded on a Bruker Tensor 27 FTIR spectrometer at room temperature with a sample chamber that was continuously purged with CO<sub>2</sub>-free dry air. Samples were equilibrated inside the instrument sample chamber for 15 min to allow purging of water vapor and CO<sub>2</sub> prior to data collection. One thousand scans were collected for each sample and buffer spectrum from 2250 to 1900 cm<sup>–1</sup> at a nominal resolution of 2 cm<sup>–1</sup>. Baseline subtraction and spectral analysis were performed using the GRAMS AI Spectroscopy Software (Thermo).

## RESULTS

**Steady State Kinetics.** The catalytic activity of all three variants (H107A, H108A, and M109I) was measured under saturating conditions of ascorbate and atmospheric O<sub>2</sub>, as a function of peptidylglycine substrate (dansyl-YVG), and the data fit by nonlinear regression to a standard Michaelis–Menton equation. Kinetic constants are compared with data for the WT enzyme in Table 1. The H107A and H108A have low activity which can be seen to be primarily the result of a large decrease in  $k_{cat}$ . The effect on  $K_M$  is different for the two mutants, with H108A binding the peptide substrate more tightly than WT, and H107A binding three times more weakly. Given the fact that the substrate binds in the vicinity of the M center, the effects on  $K_M$  induced by His to Ala mutation at the H center are intriguing. At the pH optimum for catalysis (5.8), the



**Table 1. Kinetic Parameters, Oxygen Coupling Ratios, and Copper Binding Stoichiometry of PHM H-Site Variants Compared with the Wild-Type Enzyme<sup>a</sup>**

variant	$K_m$ ( $\mu\text{M}$ )	$k_{\text{cat}}$ ( $\text{s}^{-1}$ )	specific activity	[dansyl YVG] per $[\text{O}_2]$	Cu:PHM
WT	8.2	13.8	25.7	$0.90 \pm 0.08$	$2.02 \pm 0.15$
M109I	11.8	4.6	13.7	$1.01 \pm 0.19$	$2.08 \pm 0.14$
H107A	3.3	0.08	0.25	$0.97 \pm 0.05$	$2.01 \pm 0.01$
H108A	19.4	0.11	0.38	$0.97 \pm 0.13$	$2.04 \pm 0.23$

<sup>a</sup>Estimated errors in kinetic constants are  $\pm 4\%$ . Values for oxygen coupling in the WT protein are from ref 15.

M109I substitution is not expected to have any effect on H-site copper coordination. However we consistently observed the somewhat puzzling result of a significant decrease in specific activity, with the major effect on  $k_{\text{cat}}$ . Addition of imidazole to the His to Ala mutants up to a concentration of 10 mM was unable to rescue catalytic activity.

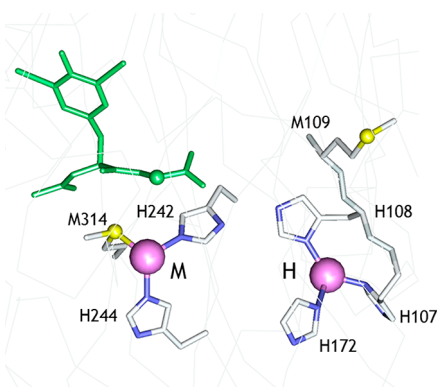


**Figure 1.** Active site structure of oxidized WT PHM (pdb file 1OPM). The substrate di-iodo-tyrosyl-glycine (I-YG) is shown in green. The H-site shows the relative orientation of the  $\text{H}^{107}\text{H}^{108}\text{M}^{109}$  motif in the active conformation, with the Met residue pointing away from the copper.

**Copper Binding.** One possibility for the dramatic decrease in catalytic rate of the H107A and H108A variants would be a loss of copper due to the loss of a critical histidine residue. Measurement of copper binding stoichiometry showed that this was not the origin of the loss of activity, since both His to Ala mutants bound Cu(II) at a ratio of close to 2:1 (Table 1). This result is comparable to that for the H172A mutant which bound Cu(II) with a ratio between 1 and 2.<sup>15,28</sup> The data suggest that loss of either H107 or H108 can be compensated by coordination of an additional ligand to complete the expected four-coordinate geometry for a cupric ion. Nevertheless, the higher binding ratios for the H107A and H108A mutants relative to H172A may indicate that H172 is more important for stabilizing the H-site structure. The contiguous positioning of H107 and H108 on the same  $\beta$ -strand constrains these ligands to coordinate via their  $\text{N}\delta$  donor atoms, which may introduce strain into the four-coordinate  $(\text{His})_3(\text{OH}_2)$  ligand set in the WT. Therefore, replacement of either H107 or H108 with a solvent ligand may result in a lower energy structure than a similar substitution at H172. The non-coordinating M109I variant reconstitutes with two Cu(II) per protein as predicted for the presence of all three coordinating His residues.

**Characterization of the Cu(II) Centers by XAS and EPR.** To gain further insight into the effects of the substitutions, we carried out EPR and XAS studies on the oxidized forms. X-band EPR spectra for WT, H107A, H108A, and M109I at pH 5.5 are shown in Figure 2. All four spectra are extremely similar

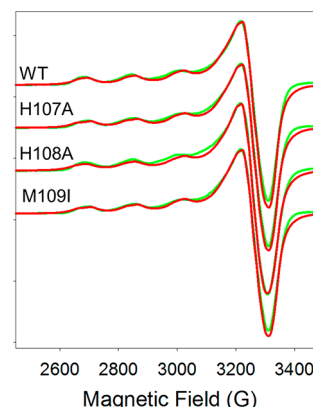


**Figure 2.** Comparison of the EPR spectra of WT PHM with its H-site variants H107A, H108A, and M109I. Red lines represent experimental data, and green lines represent simulated data using SIMPIP. Parameters used in the fits are listed in Table 2.

and despite the 11 Å separation are typical of isolated mononuclear cupric centers with little or no dipolar coupling as found previously for members of this family of enzymes.<sup>9,12,13,44</sup> Simulations using the program SIMPIP<sup>45–47</sup> gave the best fits when two axially symmetric sites were included in a 1:1 ratio, as expected for the two nonequivalent H and M sites in PHM. The  $g$ - and  $A$ -values for each site are listed in Table 2. The two sites differ slightly, with site 1 being more axial and having higher  $g_z$  and  $A_z$  values than site 2. Site 1 is most likely assigned to the M-center as the higher  $g$ - and  $A$ -values suggest more O-donor ligands (solvent) and fewer N-donors (His) than site 2. In line with this assignment, site 1 for the H107A and H108A variants does not change significantly, while the  $g_z$  and  $A_z$  values for site 2 increase slightly, as predicted by the substitution of a histidine by solvent. Alternatively, the vacant position which results from the His to Ala substitution could be occupied by an endogenous protein ligand such as a main-chain amide O group. Notwithstanding these subtle changes suggested by the simulations, the EPR parameters for the His to Ala variants are remarkably similar to WT, and rule out large changes in coordination geometry as the result of histidine removal at the H-center.

The copper coordination was also explored using X-ray absorption spectroscopy (XAS). Figure 3 (top) shows a coplot of the EXAFS of the WT and all three variants. The spectra overlay exactly, with differences less than the level of noise in the data. Simulations of the spectra (Table S1) confirm the result obtained by inspection of the four data sets, namely, that they give rise to almost identical parameters and correspond to the average coordination of 4N/O ligands per Cu(II) center, reported previously for DBM,<sup>10</sup> PHM,<sup>26</sup> and TBM.<sup>2</sup> This is not unexpected since distinguishing features arising from the substitution of one histidine in five (averaged over both copper centers) would only be observable in the shape and/or intensity of the outer-shell features at  $R = 2.8\text{--}4.3$  Å, which are the signatures of imidazole coordination. Figure 3 (bottom panel) shows a comparison of the Fourier transforms of the WT

**Table 2.** EPR Parameters Derived from Simulations to the X-Band EPR Spectra of WT, H107A, H108A, and M109I at pH 5.5<sup>a</sup>

	$g_x$	$g_y$	$g_z$	$A(x,y)$	$A(z)$	$W(x,y)$	$W(z)$
WT- site 1	2.051	2.069	2.310	18	533	49	106
site 2	2.042	2.083	2.279	25	510	49	94
H107A- site 1	2.051	2.069	2.309	18	526	49	105
site 2	2.044	2.082	2.289	25	521	49	93
H108A-site 1	2.052	2.070	2.312	18	536	49	128
site 2	2.043	2.085	2.283	25	528	49	110
M109I- site 1	2.051	2.069	2.308	18	531	49	107
site 2	2.041	2.082	2.279	25	510	49	96

<sup>a</sup>Instrumental parameters were as follows: Microwave frequency 9.400, modulation amplitude 4 G, microwave power 2 mW, temperature 100 K. No account was taken of differences in nuclear magnetic moments of 63- and 65-Cu isotopes. Line shapes were Lorentzian in all cases.

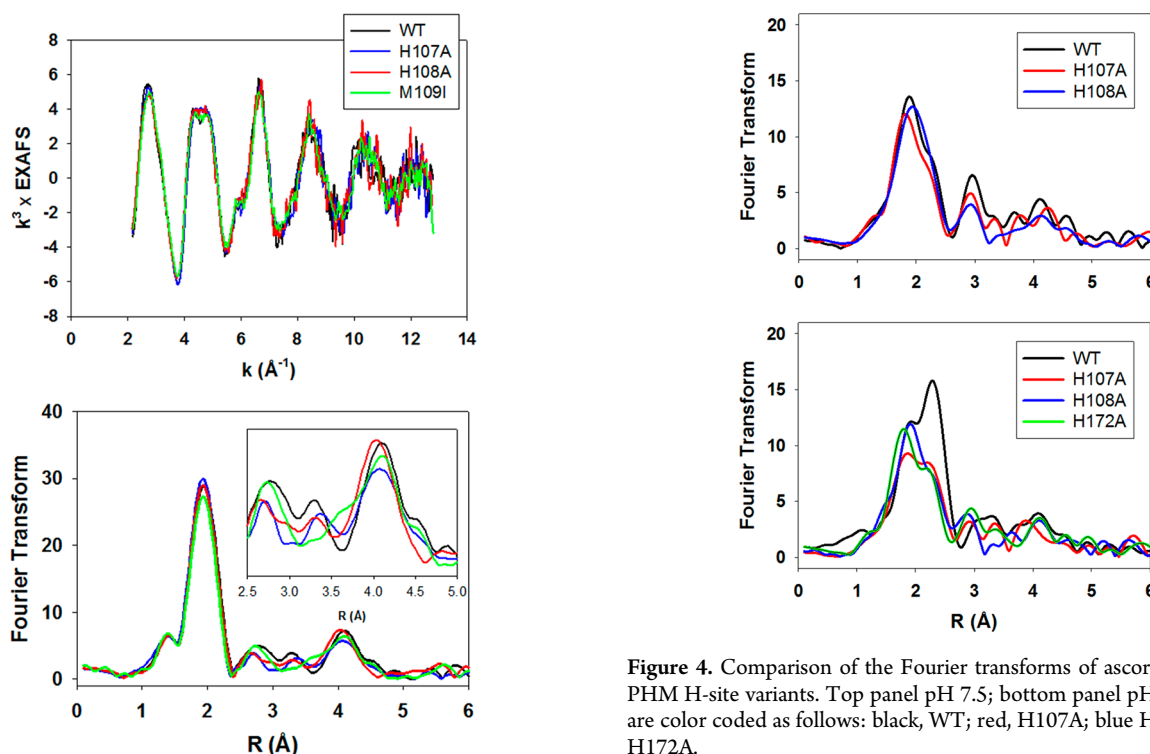


**Figure 3.** Top, overlay of the experimental EXAFS of oxidized PHM variants. Black trace, WT; blue trace, H107A; red trace H108A; green trace M109I. Bottom, overlay of experimental Fourier transforms color-coded as for the EXAFS above. The inset shows an expanded view of the imidazole outer-shell region of the transform.

protein with the three variants, from which it is evident that the intensities of the shell around 3 Å do appear to correlate with the loss of imidazole intensity in the H107A and H108A mutants. However, the trend is much less obvious in the 4 Å shell, where multiple scattering contributions dominate,<sup>48</sup> and small differences in imidazole orientation can result in greater intensity shifts than coordination numbers themselves. The EXAFS data therefore confirm conclusions derived from EPR, that the H-site His residue in H107A and H108A is replaced by coordinated solvent or an endogenous protein O/N ligand and does not perturb the coordination geometry of the site in an observable fashion.

**XAS Studies on the Reduced Proteins.** Copper coordination in the reduced proteins was probed by XAS. Figure 4 (top panel) compares the Fourier transforms for WT, H107A, and H108A at pH 7.5. The data show more complex behavior than predicted solely on the basis of histidine shell

**Figure 4.** Comparison of the Fourier transforms of ascorbate-reduced PHM H-site variants. Top panel pH 7.5; bottom panel pH 3.5. Spectra are color coded as follows: black, WT; red, H107A; blue H108A; green H172A.

occupancy with both intensities and peak positions changing, albeit with shell occupancy decreasing by less than the predicted 20%. These data can be simulated (Table 3) with the expected histidine coordination numbers, and Cu–N bond lengths ranging between 1.95 Å for the WT and 1.88 Å for the H108A variant and are broadly consistent with the trend toward a two-coordinate site at Cu<sub>H</sub>. A similar trend was observed previously in a study of the H172A variant<sup>28</sup> (included in Table 3 for comparison) where the average Cu–N(His) bond length also decreased toward the value (1.87–1.89 Å) expected for a two-coordinate bis-imidazole Cu(I) complex.<sup>29</sup> However, in contrast to H172A, the absorption edges of the H107A and H108A (Figure 5) do not show the expected increase in intensity of the 8983 eV edge feature associated with a linear two-coordinate Cu(I) complex<sup>29,49–51</sup> suggesting that the two-coordinate H-centers in H107A and H108A are significantly distorted from linearity. The data all show the presence of 0.5 Cu–S due to M314 coordination at the M-center, but interestingly, the Cu–S distance appears to decrease by ~0.04 Å in H107A and H108A relative to the WT protein. This may suggest that intersite cross-talk may influence H and M individual site structure in subtle ways that are difficult to extract from the average coordination as determined

Table 3. Parameters Used in the Simulation of the EXAFS of the H-Site Variants of PHM

	$F^a$	No <sup>b</sup>	R (Å) <sup>c</sup>	DW (Å <sup>2</sup> )	No <sup>b</sup>	R (Å) <sup>c</sup>	DW (Å <sup>2</sup> )	No <sup>b</sup>	R (Å) <sup>c</sup>	DW (Å <sup>2</sup> )	−E <sub>0</sub>
			Cu–N(His) <sup>d</sup>			Cu–O/N <sup>e</sup>			Cu–S		
Oxidized Proteins pH 7.5											
WT	0.318	2.5	1.97	0.0123	1.5	1.97	0.0123				4.69
H107A	0.316	2.0	1.96	0.0123	2.0	1.96	0.0123				5.21
H108A	0.447	2.0	1.97	0.0129	2.0	1.97	0.0129				4.95
H172A <sup>f</sup>	0.167	2.0	1.96	0.0120	2.0	1.96	0.0120				
M109I	0.287	2.5	1.97	0.0137	1.5	1.97	0.0137				−4.30
Reduced Proteins pH 7.5											
WT	0.373	2.5	1.92	0.0175				0.5	2.24	0.0123	0.34
H107A	0.487	2.0	1.88	0.0156				0.5	2.20	0.0123	−0.57
H108A	0.360	2.0	1.91	0.0152				0.5	2.20	0.0101	−0.03
H172A <sup>f</sup>	0.379	2.0	1.90	0.0130				0.5	2.23	0.0200	
M109I	0.373	2.5	1.95	0.0150				0.5	2.21	0.0094	0.26
Reduced Proteins pH 3.5											
WT	0.327	2.5	1.95	0.0182				1.0	2.26	0.0102	−0.66
H107A	0.860	2.0	1.91	0.0194				0.6	2.23	0.0120	−0.26
H108A	0.629	2.0	1.91	0.0147				0.5	2.22	0.0120	0.24
H172A <sup>f</sup>	0.659	2.0	1.88	0.0165				0.6	2.22	0.0124	−0.67
M109I	0.280	2.5	1.93	0.0159				0.5	2.21	0.0139	−0.15

<sup>a</sup> $F$  is a least-squares fitting parameter defined as  $F^2 = 1/N \sum_i k^6 (\text{Data} - \text{Model})^2$ . <sup>b</sup>Coordination numbers are generally considered accurate to  $\pm 25\%$ . <sup>c</sup>In any one fit, the statistical error in bond-lengths is  $\pm 0.005$  Å. However, when errors due to imperfect background subtraction, phase-shift calculations, and noise in the data are compounded, the actual error is closer to  $\pm 0.02$  Å. <sup>d</sup>Fits modeled histidine coordination by an imidazole ring, which included single and multiple scattering contributions from the second shell (C2/C5) and third shell (C3/N4) atoms respectively. The Cu–N–C<sub>x</sub> angles were as follows: Cu–N–C2 126°, Cu–N–C3 126°, Cu–N–N4 163°, Cu–N–C5 163°. <sup>e</sup>Distances of the Cu–N(His) and Cu–N/O (non-His) shells were constrained to be equal in fits to the oxidized proteins. <sup>f</sup>Data from ref 28.

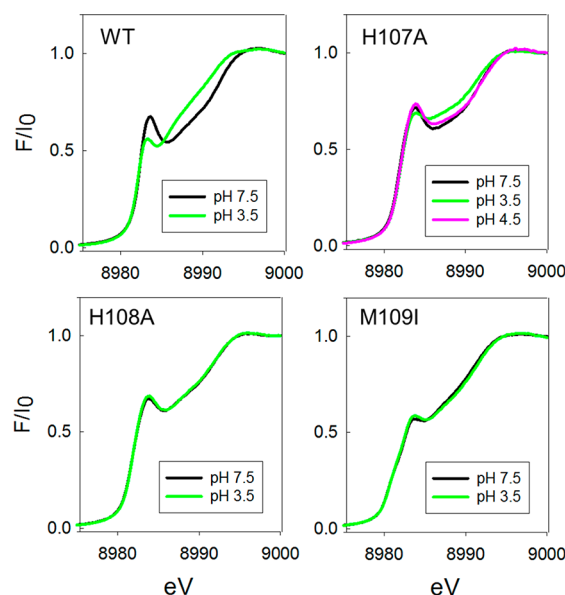


Figure 5. Comparison of absorption edges of ascorbate-reduced PHM H-site variants at neutral and low pH.

by EXAFS analysis. Notwithstanding these uncertainties, it is clear that all the H-site single His variants adopt a two-coordinate configuration with variable degrees of distortion from linearity. Fits to the EXAFS and FTs of these variants at pH 7.5 are given in Table S2 (Supporting Information).

For the WT protein, M109 does not coordinate at pH 7.5 so that the H-site of M109I is expected to be similar to that of WT at this pH. The EXAFS and FT of M109I at pH 7.5 is shown in the top panel to Figure 6, and the spectral parameters extracted from simulations are listed in Table 3. These data confirm that M109I can be simulated with all three His ligands coordinated

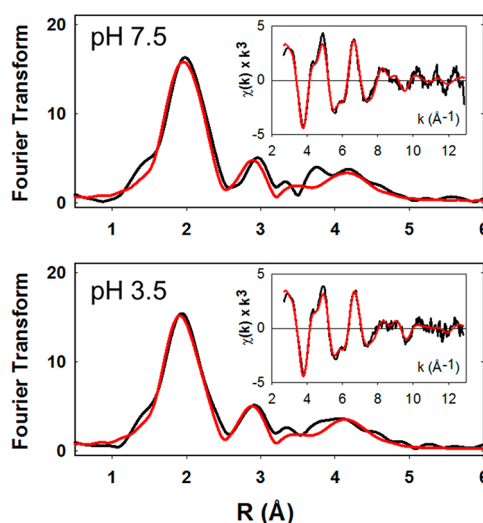


Figure 6. pH dependence of the EXAFS and Fourier transforms of the M109I variant. Black traces are experimental data, and red traces are simulated data. The top panel represents data collected at pH 7.5, and the bottom panel is data collected at pH 3.5.

at the H-site (average 2.5 over both copper centers), with a longer Cu–N(His) bond length of 1.95 Å similar to the WT protein. However, the Cu–S bond length has decreased to 2.21, which may signal some perturbation at the M-center, as the result of removal of the methionine side chain. While the decrease in  $R_{\text{Cu–S}}$  is close to the limit of detection, we note that this intriguing result could be related to the unexpected ca. 40% decrease in catalytic activity also observed for this variant.

**pH Dependence and the Role of M109 in the Low-pH Transition.** Our previous studies have suggested that the decrease in activity at low-pH is due to a conformational

change induced by a protonation event with  $pK_A$  of 4.6–4.7 which results in the coordination of an additional Met ligand at one or other of the two coppers.<sup>27</sup> On the basis of observation of similar behavior in the homologue TBM, and sequence comparisons between PHM, TBM, and DBM, we proposed that M109 was the likely origin of the low-pH Met ligand and that the conformational change was initiated by protonation of one of the His ligands at the H-center. The hypothesis leads to two predictions (i) M109I should show no decrease in catalytic activity at low pH, and (ii) the Met-off to Met-on transition should be absent in M109I. These predictions were tested by measuring the pH dependence of both the catalytic activity and the EXAFS-derived H-site coordination of the M109I variant.

Figure 7a compares the pH–activity profile of M109I with that of the WT enzyme. Differences in catalytic rate were

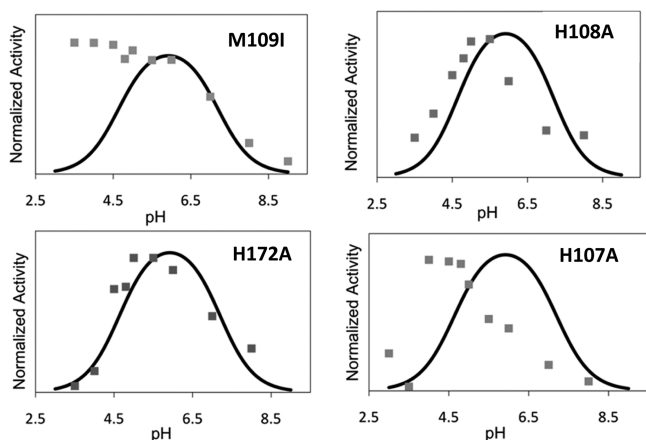


**Figure 7.** pH–rate profiles for PHM H-site variants M109I, H108A, H172A, and H107A. Rates were measured using the standard assay conditions at the different pHs as described in the text. To aid in comparison to the WT protein, all rate data have been normalized to unity, despite large differences in activity (as shown in Table 1). The solid trace in each panel is the simulated rate profile for the WT enzyme as determined in ref 27.

factored out by normalizing the rate to unity at the pH optimum of the WT enzyme so that changes in pH-dependence of the rate profile were directly comparable. In the figure, the data for WT are represented by the solid black line which corresponds to the simulation of the WT rate versus pH data published previously.<sup>27</sup> The data provide a dramatic confirmation of the prediction, viz that in M109I the rate remains high as the pH decreases below 5.5, and may actually increase in the pH range 5.5–3.0. In a second set of experiments, we compared the EXAFS of M109I at pH 7.5 and 3.5 as shown in Figure 6. The spectrum at pH 3.5 (Figure 6 bottom panel) is identical to that at pH 7.5 and lacks the increased intensity at 2.3 Å due to the additional Cu–S(Met) ligand, which is the hallmark of the low-pH structural transition (see Figure 4 bottom panel and ref 27). These data confirm our second prediction, namely, that the low-pH Cu–S(Met) interaction is eliminated in the M109I variant. Therefore, we can state with confidence that M109 coordinates via its thioether S atom in the low-pH form.

An unanswered question is the origin of the group which protonates. Previously we argued that a  $pK_A$  of 4.6 was consistent with protonation of the coordinated  $N_\delta/N_\epsilon$  of the imidazole side chain of a histidine ligand. This in turn leads to the prediction that mutation of the protonatable His residue

might also induce the conformational change and result in a species which exhibited the met-on form at all pHs. The EXAFS of H107A and H108A at pH 7.5 (Figure 4 top panel) do not show this behavior. Perhaps surprisingly, the mutations also abrogate M109 coordination at pH 3.5 as shown in Figure 4 (bottom) and Table 3. Additionally, it might be anticipated that mutation of the protonatable His residue would also abrogate the decrease in activity at low pH, producing instead an enzyme form with minimal activity over the entire pH range. Data on the pH–activity profiles of the H-site His to Ala variants are shown in Figure 7. H172A shows behavior almost identical to WT, while H108A shows a slight shift in pH optimum to lower pH values. H107A, on the other hand, shows a pH–rate profile that more closely resembles that of M109I. This would imply that H107 is the ligand that protonates since its absence abrogates M109 coordination and the associated decrease in catalytic rate, although it is still unclear why the other His variants do not show M109 Cu–S interaction in their low-pH EXAFS spectra.

**CO Binding to WT and M109I at Low pH.** CO binds to WT enzyme at pH 5.5 and above to generate an M-site carbonyl complex which has been characterized by FTIR<sup>11,37</sup> and crystallography.<sup>7</sup> The  $C\equiv O$  stretching frequency is 2092  $cm^{-1}$  which is consistent with a binding site comprised of two His, one S(Met), and CO.<sup>11,12,37</sup> To gain further insight into the coordination changes at low-pH, we used FTIR to compare the CO-binding chemistry of the WT and the H-site variants at pH 7.5 and pH 3.5. These data are shown in Figure 8. As expected, all proteins show the 2092  $cm^{-1}$  band associated with the M-site carbonyl at both pHs. However, a new band is observed at 2110  $cm^{-1}$  in the WT protein that is absent in M109I, and we therefore assign this band to an H-site carbonyl coordinated by the thioether of M109, two His residues, and the CO. This ligand set is identical to that of the M-site CO complex, yet its  $\nu(CO)$  is 20  $cm^{-1}$  higher, suggestive of weaker back-bonding into the  $\pi^*$  orbitals on the CO ligand. At present we have no explanation for the differences in frequency, but the low-pH carbonyl and its absence in M109I adds confidence to the assignment of M109 as the coordinating ligand in the low-pH H-site structure. The IR of the H107A and H108A variants at pH 3.5 also shows some intensity at 2110  $cm^{-1}$ , but of much lower intensity than the WT protein. This may suggest that a small population of H107A and H108A molecules exists in the thioether-bound conformation or that CO induces a small shift toward this conformation.

## DISCUSSION

Our data establish that mutation of any one of the three His residues at the H-center of PHM reduces activity to detectable yet extremely low levels. Most of the loss is associated with  $k_{cat}$ , although  $K_M$  varies by a factor of 3 with H107A having the highest affinity and H108A the lowest. This loss of activity is not due to inability to bind Cu in either the oxidized or reduced states. Furthermore, the structures as visualized by EPR and EXAFS spectroscopy appear similar in all cases to those observed in the WT fully active enzyme. In the oxidized mutant proteins, solvent appears competent to bind in place of imidazole to generate four- or five-coordinate H-site structures, whereas in the reduced proteins any two histidine residues appear competent to bind Cu(I), albeit with some indication from absorption edge intensities of different degrees of distortion from linearity. Since H107 and H108 are contiguous residues on the same  $\beta$ -strand, they are constrained to bind in a



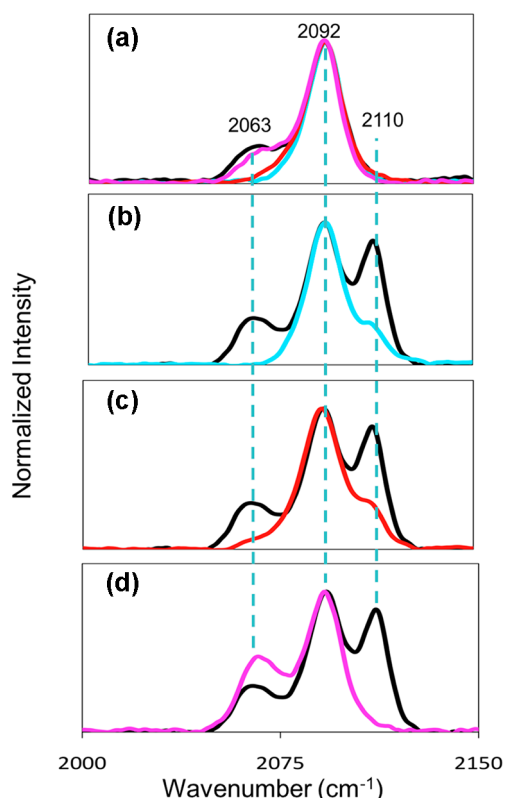


**Figure 8.** FTIR spectra of the CO complexes of WT PHM and its H-site variants in the C≡O stretching region. (a) Comparison of IR spectra at pH 7.5 for WT (black), H107A (cyan), H108A (red), and M109I (magenta); (b–d) comparison of IR spectra at pH 3.5 for WT (black) and H107A (cyan) (b); WT (black) and H108A (red) (c); WT (black) and M109I (magenta) (d). Spectra are normalized to the intensity of the WT 2092  $\text{cm}^{-1}$  band.

*trans*-configuration via their N $\delta$  imidazole N atoms and hence are likely most stable in linear two-coordinate geometry.<sup>49</sup> This was previously noted in an earlier study of the H172A variant where a significant increase in absorption edge intensity (characteristic of two-coordinate linear geometry<sup>29,50</sup>) was observed. For the H107A and H108A variants, the 8983 eV intensity was not significantly increased above that found in the WT protein, suggesting that these variants may be unable to reorient so as to adopt the thermodynamically preferred linear structure. This observation, coupled to the almost complete loss of activity in single H-site variants, may suggest that the H-site is built on a fairly rigid scaffold where precise orientation of His ligands is an essential element of function.

It is puzzling that solvent readily substitutes for the missing imidazole side chain, yet exogenous ligands do not appear to bind at H. Azide, nitrite, and peroxide bind exclusively to the M-center in the oxidized protein, while CO binds to M in the reduced form.<sup>7,8,11–13,37</sup> Likewise addition of imidazole to any of the H-site His to Ala mutants fails to rescue activity (ref 28 and this work). This may be due to a lack of reactivity (similar to azide), but it may also support the hypothesis advanced above that H-site reactivity is intimately involved with the connectivity of the His ligands to the protein scaffold, which either completes ET circuitry or organizes other key elements of structure. It is noteworthy that the X-ray crystal structure of the M-site M314I mutant shows a highly perturbed H-site structure with H107 completely dissociated.<sup>6</sup> The cross-talk between H and M implied by this structure is also manifest in

changes in the  $K_M$  for substrate binding of H-site mutants, even though the substrate binds at a site many angstroms distant. Thus, subtle changes in the H-site structure may propagate through the scaffold to M, where they could inhibit the enzyme from achieving critical conformations necessary for H-tunneling.<sup>52,53</sup>

The pH dependence of catalytic activity gives further insight into protonation/deprotonation events that interconvert active and inactive states. In this study, we have focused on the protonation event that generates an inactive state with a  $pK_A$  of 4.6.<sup>27,39</sup> Our earlier work advanced the hypothesis that pH induced a conformational switch between a catalytically competent active state of the H-center and an inactive state containing a new Cu–S ligand. We further speculated that the new S residue was derived from the side chain of M109, which is part of the H-site conserved HHM motif but points away from Cu<sub>H</sub> on the opposite side of the  $\beta$ -strand (Figure 1). The hypothesis allowed us to make two predictions (i) that the absence of a thioether at residue 109 would prevent the M109 S(Met) coordination thereby attenuating the driving force for this conformational switch, and (ii) that its absence would therefore eliminate the loss of activity at low pH. Both of these predictions were borne out by the data. The M109I variant showed a small increase in activity in the pH range 5.5–3.0 and lacked the high-intensity Cu–S interaction characteristic of the low-pH state of the WT enzyme. This allows us to conclude with confidence that in the WT enzyme, the low-activity state has undergone a conformational switch which flips the  $\beta$ -sheet, repositioning the coordinating ligands such that M109 is in a favorable orientation to bind to Cu<sub>H</sub>.

The observed  $pK_A$  for the catalytic transition of 4.6 is within the range expected for protonation of histidine residues coordinated to Cu(I). Well established cases of this behavior include the reduced forms of cupredoxins<sup>54,55</sup> and Cu/Zn superoxide dismutases,<sup>56–58</sup> where protonation is coupled to addition of an electron so as to keep the overall charge constant. As noted previously,<sup>27</sup> the C-terminal histidine ligand of the cupredoxin site is located in a loop of sequence between the Cys112 and Met121 (azurin numbering), and the  $pK_A$  for histidine protonation is sensitive to both the identity and length of the sequence<sup>59</sup> with values ranging from 2 to 6. For example, replacement of the native loop of azurin (C<sup>112</sup>TFPGH<sup>117</sup>SALM,  $pK_A^{\text{H}117} < 2$ ) with shorter loops from amicyanin or plastocyanin produces chimeras with  $pK_A$ 's for protonation of the corresponding histidine of 5.5 and 4.3 respectively, while for plastocyanin, the  $pK_A$ 's of the native protein and the chimera in which the native loop (C<sup>84</sup>SPH<sup>87</sup>QGAGM<sup>92</sup>) is replaced with the azurin loop-sequence are 4.7 and 4.9. We reasoned that if protonation of an H-site coordinating histidine was responsible for the conformational switch, then its mutation to alanine should either eliminate or at least strongly perturb both the pH-rate profile and the structural transition leading to S(Met) binding. The data show that H172A exhibits the WT pH-rate profile, while H108A has a rate profile only slightly shifted to lower pH. H107A on the other hand has a strongly perturbed rate profile which approximates that of M109I showing an increase in rate between 5.5 and 4, below which the activity crashes to zero. Additionally, close inspection of the EXAFS data suggests an increase in Cu–S site occupancy for H107A to 0.65 at pH 3.5, while FTIR shows evidence for the S-coordinated H-site carbonyl (2010  $\text{cm}^{-1}$ ). These observations may suggest an equilibrium between M109-on and -off states in H107A and leads us to propose that H107 is



the residue which protonates. The inability of the H107A mutant to induce a complete conformational switch was at first puzzling, as the prediction was that the absence of the protonating residue would generate the Met109-on state at all pHs. However, further analysis suggests that the switch may be driven by the replacement of the coordinating histidine by its bulky noncoordinating protonated form and is induced by a combination of S(M109) coordination and relief of steric crowding. In this model, the hole created by the Ala substitution would create no steric restrictions and could therefore be a stable entity at all pHs. We also note that H107A does not appear to protonate as readily in the M109I variant, as no decrease in activity is observed with M109I between pH 6 and 3. This observation implies that the  $pK_A$  for His protonation is coupled to the ability of the Met ligand to coordinate: without the driving force for S ligation, Cu(I) outcompetes the proton for histidine binding.

The M109-on state of the enzyme is catalytically incompetent, and the obvious next question is why. Binding of CO to the low pH inactive (S-bound) form of the WT enzyme induces a new band at  $2110\text{ cm}^{-1}$ , absent in the M109I variant, which we may logically assign to a four-coordinate H-site carbonyl with two histidines, one methionine, and CO. On the other hand, the active state of the H-site does not form a CO complex. These observations give hints to the possible geometrical differences between active and inactive states. Cu(I) carbonyls are generally formed from three-coordinate precursors to give predominately four-coordinate tetrahedral complexes<sup>51,60,61</sup> and react poorly if at all with two-coordinate Cu(I) complexes. A recent study of an H-site PHM model peptide containing the HH motif confirmed this chemistry: the two-coordinate Cu(I)-N $\delta$ ,N $\delta$ -bis-imidazole complex reacted sluggishly with CO to generate a weak three-coordinate CO complex with a low-intensity  $\nu(\text{C}\equiv\text{O})$  between 2105 and  $2110\text{ cm}^{-1}$ . However, in the presence of an additional mol equiv of imidazole, the four-coordinate Cu(I)(His) $_3$ CO species was formed stoichiometrically and exhibited a strong  $\nu(\text{C}\equiv\text{O})$  at lower frequency ( $2075\text{ cm}^{-1}$ ) as expected.<sup>29</sup> With regard to the low pH WT PHM spectrum, it is possible that the  $2110\text{ cm}^{-1}$  is due to a Cu(I)(His) $_2$ CO structure, but the strong intensity of the band together with its absence in the M109I variant suggests that the four-coordinate Cu(I)(His) $_2$ S(Met)CO species is more likely. We believe that the assignment is reasonable since the thioether ligand is a poor donor and hence may have little impact on the extent of back bonding.

The question remains, if the low activity S-bound H-site readily forms a carbonyl, why not the three-coordinate high activity site? The answer must lie in the ability of lack thereof of the three-coordinate precursor to rearrange on CO binding to a tetrahedral coordination. This again suggests that a rigid protein scaffold associated with the H-site active form may be required for electron transfer.

Most cuproproteins including PHM and DBM are packaged into vesicles in the TGN as folded apo-proteins that still require metalation. This function is performed by copper transporting ATPases<sup>62–65</sup> which are members of the P1B family of heavy metal transporters found in all forms of life from bacteria to mammals where they function in copper export across membranes. Mammalian ATP7A resides in the TGN or vesicular membranes and pumps copper from the cytosolic to the luminal side of the membrane where it is believed to transfer copper directly to PHM without the intermediacy of an intravesicular copper chaperone.<sup>66</sup> ATP7A contains a luminal

loop rich in His and Met residues (MDHHFAT-LHHNQNMSSKEEMINLHSSM)<sup>67,68</sup> which has been shown to bind Cu(I) at pH 8 with two-coordinate (His) $_2$  ligation and weak additional interaction with a Met residue.<sup>69</sup> On the basis of *in vitro* data, it was postulated that this loop binds copper as it exits the membrane channel, and passes it onto cuproproteins such as PHM which are also associated with the luminal membrane.<sup>62</sup> As the vesicles mature, their pH drops as the result of H $^+$  import, resulting in an internal pH of  $\sim 5.5$ , close to the pH optimum of the monooxygenases with the consequence that the ATP7A luminal loop is subject to the same pH constraints as its putative PHM partner. At present, the effect of pH on the Cu(I)-binding properties of the loop has not been investigated, but it is intriguing that similar HM signals appear to be present in both systems, suggesting that HHX $_n$ M motifs may have more general utility as Cu-dependent conformational switches that could modulate coordination in response to pH. Further studies are underway to explore this and other aspects of HHM chemistry.

## ■ ASSOCIATED CONTENT

### ● Supporting Information

Two figures and one table are available free of charge via the Internet at <http://pubs.acs.org>.

## ■ AUTHOR INFORMATION

### Corresponding Author

\*Phone: (503)748-1384. Fax: (503)748-1464. E-mail: [ninian@comcast.net](mailto:ninian@comcast.net).

### Funding

This work was supported by a grant from the National Institutes of Health (R01 NS027583) to N.J.B. We gratefully acknowledge the use of facilities at the Stanford Synchrotron Radiation Lightsource which is supported by the National Institutes of Health Biomedical Research and Technology Program Division of Research Resources and by the U.S. Department of Energy Office of Biological and Environmental Research.

### Notes

The authors declare no competing financial interest.

## ■ ACKNOWLEDGMENTS

We thank Drs. Betty Eipper and Richard Mains for the gift of cell lines for the WT and H107A PHM proteins.

## ■ ABBREVIATIONS USED

MES, 2-(*N*-morpholino)ethanesulfonic acid; HEPES, 4-(2-hydroxyethyl)-1-piperazine-ethanesulfonic acid; CHES, *N*-cyclohexyl-2-aminoethanesulfonic acid; dansyl-YVG, dansyl-Tyr-Val-Gly; PHM, peptidylglycine monooxygenase; EXAFS, extended X-ray absorption fine structure; XAS, X-ray absorption spectroscopy; HPLC, high pressure liquid chromatography; ICP-OES, inductively coupled plasma optical emissions spectrometry; DBM, dopamine  $\beta$ -monooxygenase; TBM, tyramine  $\beta$ -monooxygenase; TFA, trifluoroacetic acid; TCA, trichloroacetic acid; WT, wild-type; *Dhfr*, dihydrofolate reductase gene; CHO, chinese hamster ovary; DMEM F-12, Dulbecco's modified Eagle's medium; FBS FCI, fetal clone II; SDS-PAGE, sodium dodecyl sulfate polyacrylamide gel electrophoresis; PBS, phosphate buffer saline; ECS, extra capillary space; MWCO, molecular weight cut off

# REFERENCES

- (1) Klinman, J. P. (2006) The copper-enzyme family of dopamine b-monooxygenase and peptidylglycine a-hydroxylating monooxygenase: Resolving the chemical pathway for substrate hydroxylation. *J. Biol. Chem.* 281, 3013–3016.
- (2) Hess, C. R., Klinman, J. P., and Blackburn, N. J. (2010) The copper centers of tyramine beta-monooxygenase and its catalytic-site methionine variants: an X-ray absorption study. *J. Biol. Inorg. Chem.* 15, 1195–1207.
- (3) Prigge, S. T., Mains, R. E., Eipper, B. A., and Amzel, L. M. (2000) New insights into copper monooxygenases and peptide amidation: structure, mechanism and function. *Cell. Mol. Life Sci.* 57, 1236–1259.
- (4) Prigge, S. T., Kolhekar, A. S., Eipper, B. A., Mains, R. E., and Amzel, L. M. (1997) Amidation of bioactive peptides: the structure of peptidylglycine a-hydroxylating monooxygenase. *Science* 278, 1300–1305.
- (5) Prigge, S. T., Kolhekar, A. S., Eipper, B. A., Mains, R. E., and Amzel, L. M. (1999) Substrate-mediated electron transfer in peptidylglycine a-hydroxylating monooxygenase. *Nat. Struct. Biol.* 6, 976–983.
- (6) Siebert, X., Eipper, B. A., Mains, R. E., Prigge, S. T., Blackburn, N. J., and Amzel, L. M. (2005) The catalytic copper of peptidylglycine alpha-hydroxylating monooxygenase also plays a critical structural role. *Biophys. J.* 89, 3312–3319.
- (7) Chufan, E. E., Prigge, S. T., Siebert, X., Eipper, B. A., Mains, R. E., and Amzel, L. M. (2010) Differential reactivity between two copper sites in peptidylglycine alpha-hydroxylating monooxygenase. *J. Am. Chem. Soc.* 132, 15565–15572.
- (8) Rudzka, K., Moreno, D. M., Eipper, B., Mains, R., Estrin, D. A., and Amzel, L. M. (2013) Coordination of peroxide to the Cu(M) center of peptidylglycine a-hydroxylating monooxygenase (PHM): structural and computational study. *J. Biol. Inorg. Chem.* 18, 223–232.
- (9) Hess, C. R., Wu, Z., Ng, A., Gray, E. E., McGuirl, M. A., and Klinman, J. P. (2008) Hydroxylase activity of Met471Cys tyramine b-monooxygenase. *J. Am. Chem. Soc.* 130, 11939–11944.
- (10) Blackburn, N. J., Hasnain, S. S., Pettingill, T. M., and Strange, R. W. (1991) Copper K-EXAFS studies of oxidized and reduced dopamine-b-hydroxylase: confirmation of a sulfur ligand to Cu(I) in the reduced enzyme. *J. Biol. Chem.* 266, 23120–23127.
- (11) Pettingill, T. M., Strange, R. W., and Blackburn, N. J. (1991) Carbonmonooxygenase dopamine-b-hydroxylase: structural characterization by FTIR, fluorescence and XAS spectroscopy. *J. Biol. Chem.* 266, 16996–17003.
- (12) Boswell, J. S., Reedy, B. J., Kulathila, R., Merkle, D. J., and Blackburn, N. J. (1996) Structural investigations on the coordination environment of the active-site copper centers of recombinant bifunctional peptidylglycine a-amidating enzyme. *Biochemistry* 35, 12241–12250.
- (13) Chen, P., Bell, J., Eipper, B. A., and Solomon, E. I. (2004) Oxygen activation by the noncoupled binuclear copper site in peptidylglycine a-hydroxylating monooxygenase. Spectroscopic definition of the resting sites and the putative CuII<sub>M</sub>-OOH intermediate. *Biochemistry* 43, 5735–5747.
- (14) Evans, J. P., Ahn, K., and Klinman, J. P. (2003) Evidence that dioxygen and substrate activation are tightly coupled in dopamine b-monooxygenase: Implications for oxygen activation. *J. Biol. Chem.* 278, 49691–49698.
- (15) Evans, J. P., Blackburn, N. J., and Klinman, J. P. (2006) The catalytic role of the copper ligand H172 of peptidylglycine a-hydroxylating monooxygenase: a kinetic study of the H172A mutant. *Biochemistry* 45, 15419–15429.
- (16) Chen, P., and Solomon, E. I. (2004) Oxygen activation by the noncoupled binuclear copper site in peptidylglycine a-hydroxylating monooxygenase. Reaction mechanism and role of the noncoupled nature of the active site. *J. Am. Chem. Soc.* 126, 4991–5000.
- (17) Chen, P., and Solomon, E. I. (2004) O<sub>2</sub> activation by binuclear Cu sites: noncoupled versus exchange coupled reaction mechanisms. *Proc. Natl. Acad. Sci. U. S. A.* 101, 13105–13110.
- (18) Crespo, A., Marti, M. A., Roitberg, A. E., Amzel, L. M., and Estrin, D. A. (2006) The catalytic mechanism of peptidylglycine a-hydroxylating monooxygenase investigated by computer simulation. *J. Am. Chem. Soc.* 128, 12817–12828.
- (19) Magnus, K. A., Hazes, B., Ton-That, H., Bonaventura, C., Bonaventura, J., and Hol, W. G. J. (1994) Crystallographic analysis of oxygenated and deoxygenated states of arthropod hemocyanin shows unusual differences. *Proteins Struct. Funct. Genet.* 19, 302–309.
- (20) Gerdemann, C., Eicken, C., and Krebs, B. (2002) The crystal structure of catechol oxidase: new insight into the function of type-3 copper proteins. *Acc. Chem. Res.* 35, 183–191.
- (21) Matoba, Y., Kumagai, T., Yamamoto, A., Yoshitsu, H., and Sugiyama, M. (2006) Crystallographic evidence that the dinuclear copper center of tyrosinase is flexible during catalysis. *J. Biol. Chem.* 281, 8981–8990.
- (22) Lewis, E. A., and Tolman, W. B. (2004) Reactivity of dioxygen-copper systems. *Chem. Rev.* 104, 1047–1076.
- (23) Citek, C., Lyons, C. T., Wasinger, E. C., and Stack, T. D. (2012) Self-assembly of the oxy-tyrosinase core and the fundamental components of phenolic hydroxylation. *Nat. Chem.* 4, 317–322.
- (24) Prigge, S. T., Eipper, B. A., Mains, R. E., and Amzel, L. M. (2004) Dioxygen binds end-on to mononuclear copper in a precatalytic enzyme complex. *Science* 304, 864–867.
- (25) Bauman, A. T., Yukl, E. T., Alkevich, K., McCormack, A. L., and Blackburn, N. J. (2006) The hydrogen peroxide reactivity of peptidylglycine monooxygenase supports a Cu(II)-superoxo catalytic intermediate. *J. Biol. Chem.* 281, 4190–4198.
- (26) Blackburn, N. J., Rhames, F. C., Ralle, M., and Jaron, S. (2000) Major changes in copper coordination accompany reduction of peptidylglycine monooxygenase. *J. Biol. Inorg. Chem.* 5, 341–353.
- (27) Bauman, A. T., Broers, B. A., Kline, C. D., and Blackburn, N. J. (2011) A Copper-Methionine Interaction Controls the pH-Dependent Activation of Peptidylglycine Monooxygenase. *Biochemistry* 50, 10819–10828.
- (28) Jaron, S., Mains, R. E., Eipper, B. A., and Blackburn, N. J. (2002) The catalytic role of the copper ligand H172 of peptidylglycine a-hydroxylating monooxygenase (PHM): a spectroscopic study of the H172A mutant. *Biochemistry* 41, 13274–13282.
- (29) Himes, R. A., Park, Y. G., Barry, A. N., Blackburn, N. J., and Karlin, K. D. (2007) Synthesis and X-ray absorption spectroscopy structural studies of Cu(I) complexes of histidylhistidine peptides: The predominance of linear 2-coordinate geometry. *J. Am. Chem. Soc.* 129, 5352–5353.
- (30) Osborne, R. L., Zhu, H., Iavarone, A. T., Blackburn, N. J., and Klinman, J. P. (2013) Interdomain Long-Range Electron Transfer Becomes Rate-Limiting in the Y216A Variant of Tyramine beta-Monooxygenase. *Biochemistry* 52, 1179–1191.
- (31) Cardenas, D. J., Cuerva, J. M., Alias, M., Bunuel, E., and Campana, A. G. (2011) Water-based hydrogen-atom wires as mediators in long-range proton-coupled electron transfer in enzymes: a new twist on water reactivity. *Chemistry* 17, 8318–8323.
- (32) Eipper, B. A., Quon, A. S. W., Mains, R. E., Boswell, J. S., and Blackburn, N. J. (1995) The catalytic core of peptidylglycine a-hydroxylating monooxygenase: investigation by site-directed mutagenesis, Cu x-ray absorption spectroscopy, and electron paramagnetic resonance. *Biochemistry* 34, 2857–2865.
- (33) Kolhekar, A. S., Keutman, H. T., Mains, R. E., Quon, A. S. W., and Eipper, B. A. (1997) Peptidylglycine a-hydroxylating monooxygenase: active site residues, disulfide linkages, and a two-domain model of the catalytic core. *Biochemistry* 36, 10901–10909.
- (34) Horton, R. M., Cai, Z. L., Ho, S. N., and Pease, L. R. (1990) Gene splicing by overlap extension: tailor-made genes using the polymerase chain reaction. *BioTechniques* 8, 528–535.
- (35) Oyarc, A. M., Steveson, T. C., Jin, L., and Eipper, B. A. (2001) Dopamine beta-monooxygenase signal/anchor sequence alters trafficking of peptidylglycine alpha-hydroxylating monooxygenase. *J. Biol. Chem.* 276, 33265–33272.
- (36) Husten, E. J., and Eipper, B. A. (1991) The membrane-bound bifunctional peptidylglycine a-amidating monooxygenase protein.

Exploration of its domain structure through limited proteolysis. *J. Biol. Chem.* 266, 17004–17010.

(37) Jaron, S., and Blackburn, N. J. (1999) Does superoxide channel between the copper centers in peptidylglycine monooxygenase? A new mechanism based on carbon monoxide reactivity. *Biochemistry* 38, 15086–15096.

(38) Bauman, A. T., Ralle, M., and Blackburn, N. (2007) Large scale production of the copper enzyme peptidylglycine monooxygenase using an automated bioreactor. *Protein Expression Purification* 51, 34–38.

(39) Bauman, A. T., Jaron, S., Yukl, E. T., Burchfiel, J. R., and Blackburn, N. (2006) pH dependence of peptidylglycine monooxygenase. Mechanistic implications for Cu-methionine binding dynamics. *Biochemistry* 45, 11140–11150.

(40) George, G. N. (1995) EXAFSPAK, Stanford Synchrotron Radiation Laboratory, Menlo Park, CA.

(41) Binsted, N., and Hasnain, S. S. (1996) State of the art analysis of whole X-ray absorption spectra. *J. Synchrotron Radiat.* 3, 185–196.

(42) Gurman, S. J., Binsted, N., and Ross, I. (1984) A rapid, exact, curved-wave theory for EXAFS calculations. *J. Phys. C* 17, 143–151.

(43) Gurman, S. J., Binsted, N., and Ross, I. (1986) A rapid, exact, curved-wave theory for EXAFS calculations. II. The multiple-scattering contributions. *J. Phys. C* 19, 1845–1861.

(44) Blackburn, N. J., Concannon, M., Khosrow Shahiyan, S., Mabbs, F. E., and Collison, D. (1988) The active site of dopamine- $\beta$ -hydroxylase. Comparison of derivatives containing four and eight coppers per tetramer using potentiometry and EPR spectroscopy. *Biochemistry* 27, 6001–6008.

(45) Nilges, M. J. (1979) SIMPIP EPR simulation program, Illinois EPR Research Center (IERC), University of Illinois, Urbana-Champaign.

(46) Nilges, M. J., Matteson, K., and Belford, R. L. (2006) A software package for the simulation of ESR powder-type spectra, In *ESR Spectroscopy in Membrane Biophysics* (Hemminga, M. A., and Berliner, L. J., Eds.), Springer, New York.

(47) Siluvai, G. S., Mayfield, M., Nilges, M. J., DeBeer George, S., and Blackburn, N. J. (2010) Anatomy of a red copper center: Spectroscopic identification and reactivity of the copper centers of *Bacillus subtilis* Sco and its Cys-to-Ala variants. *J. Am. Chem. Soc.* 132, 5215–5226.

(48) Strange, R. W., Blackburn, N. J., Knowles, P. F., and Hasnain, S. S. (1987) X-ray absorption spectroscopy of metal-histidine coordination in metalloproteins. Exact simulation of the EXAFS of tetraimidazole-copper(II) nitrate and other copper-imidazole complexes by the use of a multiple scattering treatment. *J. Am. Chem. Soc.* 109, 7157–7162.

(49) Himes, R. A., Park, G. Y., Siluvai, G. S., Blackburn, N. J., and Karlin, K. D. (2008) Structural studies of copper(I) complexes of amyloid- $\beta$  peptide fragments: formation of two-coordinate bis-(histidine) complexes. *Angew. Chem., Int. Ed. Engl.* 47, 9084–9087.

(50) Pickering, I. J., George, G. N., Dameron, C. T., Kurz, B., Winge, D. R., and Dance, I. G. (1993) X-ray absorption spectroscopy of cuprous-thiolate clusters in proteins and model systems. *J. Am. Chem. Soc.* 115, 9498–9505.

(51) Sanyal, I., Karlin, K. D., Strange, R. W., and Blackburn, N. J. (1993) Chemistry and structural studies on the dioxygen-binding copper-1,2 dimethylimidazole system. *J. Am. Chem. Soc.* 115, 11259–11270.

(52) Francisco, W. A., Knapp, M. J., Blackburn, N. J., and Klinman, J. P. (2002) Hydrogen tunneling in peptidylglycine  $\alpha$ -hydroxylating monooxygenase. *J. Am. Chem. Soc.* 124, 8194–8195.

(53) Klinman, J. P. (2006) The role of tunneling in enzyme catalysis of C-H activation. *Biochim. Biophys. Acta* 1757, 981–987.

(54) Guss, J. M., Harrowell, P. R., Murata, M., Norris, V. A., and Freeman, H. C. (1986) Crystal structure analyses of reduced (CuI) poplar plastocyanin at six pH values. *J. Mol. Biol.* 192, 361–387.

(55) Li, C., Sato, K., Monari, S., Salard, I., Sola, M., Banfield, M. J., and Dennison, C. (2011) Metal-binding loop length is a determinant

of the pK<sub>a</sub> of a histidine ligand at a type 1 copper site. *Inorg. Chem.* 50, 482–488.

(56) Bertini, I., Luchinat, C., and Monnanni, R. (1985) Evidence of the breaking of the copper-imidazolate bridge in copper/cobalt-substituted superoxide dismutase upon reduction of the Cu(II) centers. *J. Am. Chem. Soc.* 107, 2178–2179.

(57) Blackburn, N. J., Hasnain, S. S., Binsted, N., Diakun, G. P., Garner, C. D., and Knowles, P. F. (1984) An extended-x-ray-absorption-fine-structure study of bovine erythrocyte superoxide dismutase in aqueous solution. Direct evidence for three-coordinate Cu(I) in the reduced enzyme. *Biochem. J.* 219, 985–990.

(58) Banci, L., Bertini, I., Cramaro, F., Del Conte, R., and Viezzoli, M. S. (2002) The solution structure of reduced dimeric copper zinc superoxide dismutase. The structural effects of dimerization. *Eur. J. Biochem.* 269, 1905–1915.

(59) Li, C., Banfield, M. J., and Dennison, C. (2007) Engineering copper sites in proteins: loops confer native structures and properties to chimeric cupredoxins. *J. Am. Chem. Soc.* 129, 709–718.

(60) Pasquali, M., and Floriani, C. (1984) Cu(I)-carbon monoxide chemistry: recent advances and perspectives, In *Copper Coordination Chemistry, Biochemical and Inorganic Perspectives* (Karlin, K. D., and Zubieta, J., Eds.) pp 311–330, Adenine Press, New York.

(61) Blackburn, N. J., Strange, R. W., Farooq, A., Haka, M. S., and Karlin, K. D. (1988) X-ray absorption studies of three-coordinate dicopper(I) complexes and their dioxygen adducts. *J. Am. Chem. Soc.* 110, 4263–4272.

(62) Steveson, T. C., Ciccotosto, G. D., Ma, X.-M., Mueller, G. P., Mains, R. E., and Eipper, B. A. (2003) Menkes protein contributes to the function of peptidylglycine  $\alpha$ -amidating monooxygenase. *Endocrinology* 144, 188–200.

(63) Petris, M. J., Strausak, D., and Mercer, J. F. (2000) The Menkes copper transporter is required for the activation of tyrosinase. *Hum. Mol. Genet.* 9, 2845–2851.

(64) Setty, S. R., Tenza, D., Sviderskaya, E. V., Bennett, D. C., Raposo, G., and Marks, M. S. (2008) Cell-specific ATP7A transport sustains copper-dependent tyrosinase activity in melanosomes. *Nature* 454, 1142–1146.

(65) Qin, Z., Itoh, S., Jeney, V., Ushio-Fukai, M., and Fukai, T. (2006) Essential role for the Menkes ATPase in activation of extracellular superoxide dismutase: implication for vascular oxidative stress. *FASEB J.* 20, 334–336.

(66) El Meskini, R., Culotta, V. C., Mains, R. E., and Eipper, B. A. (2003) Supplying copper to the cuproenzyme peptidylglycine  $\alpha$ -amidating monooxygenase. *J. Biol. Chem.* 278, 12278–12284.

(67) Pope, C. R., Flores, A. G., Kaplan, J. H., and Unger, V. M. (2012) Structure and function of copper uptake transporters. *Curr. Top. Membr.* 69, 97–112.

(68) Barry, A. N., Otoikhian, A., Bhatt, S., Shinde, U., Tsivkovskii, R., Blackburn, N. J., and Lutsenko, S. (2011) The Luminal Loop Met672-Pro707 of Copper-transporting ATPase ATP7A Binds Metals and Facilitates Copper Release from the Intramembrane Sites. *J. Biol. Chem.* 286, 26585–26594.

(69) Otoikhian, A., Barry, A. N., Mayfield, M., Nilges, M., Huang, Y., Lutsenko, S., and Blackburn, N. J. (2012) Luminal loop M672-P707 of the Menkes protein (ATP7A) transfers copper to peptidylglycine monooxygenase. *J. Am. Chem. Soc.* 134, 10458–10468.